scientific data

Check for updates

OPEN

DATA DESCRIPTOR

Fast Single-Particle Tracking of Membrane Proteins Combined with Super-Resolution Imaging of Actin Nanodomains

Hanieh Mazloom-Farsibaf[1,4] ✉, William K. Kanagy[2,5], Diane S. Lidke[2,3] & Keith A. Lidke[1,3] ✉

Membrane protein dynamics regulates cell functions by initiating downstream signaling cascades. The cell membrane is compartmentalized into nanodomains by actin structures, restricting lateral protein diffusion. Single-particle tracking offers high spatiotemporal resolution for studying protein dynamics in living cells. However, directly observing actin filaments that form barriers of nanodomains for fast protein diffusion is challenging due to their size being below the diffraction limit. Single-molecule localization microscopy resolves these structures but requires imaging in fixed cells. We integrated fast single-particle tracking with single-molecule localization microscopy to generate a dataset of membrane protein dynamics and actin filaments within the same cells at the nanoscales. Optimizing the fixation protocol enabled transition from live-cell tracking to fixed-cell super-resolution imaging. Data for the high-affinity IgE receptor, a transmembrane protein, and the GPI-anchored protein, an outer leaflet protein, was collected at 490 Hz. After fixation, actin filaments were imaged using dSTORM. The treatment of actin structures with phalloidin and PMA generated a dataset of distinct actin architectures for studying their potential influence on membrane protein dynamics.

Background & Summary

The cell membrane, serving as a dynamic platform for lipid and protein interactions, continuously generates signals that are essential for cellular functions[1–3]. Spatial organization of membrane proteins depends on both intrinsic biophysical properties of the membrane[4] and membrane-associated actin cytoskeleton, as proposed by the picket-fence model[5,6]. Based on this model, actin structures compartmentalize the membrane into nano-corrals and restrict membrane protein mobility. Considering Brownian motion for a membrane-associated molecule, whether a protein or lipid, with a lateral diffusion of ~0.1–1 $\mu m^2/s$, the molecule must be tracked within 2–20 milliseconds to reveal trapped diffusion within a corral of ~100 nm[7]. This compartmentalization can also result in "hop diffusion", where molecules move between connected corrals[8,9].

Previous studies, directly and indirectly, observed that actin structures underneath the membrane impact lateral diffusion of membrane components including lipids[10–12], outer leaflet proteins[13], inner raft proteins[14], and transmembrane proteins[15,16]. However, the question of whether filamentous actin, with a thickness of seven nanometers, acts as a diffusion barrier is still unrevealed. The trade-off between resolution and sampling also applies to single-molecule localization microscopy (SMLM)[17]. To detect actin structures as small as 25 nanometers, SMLM must acquire thousands of images of sparsely labeled samples, which are then reconstructed into a final super-resolution image. For our desired resolution of actin, this process requires the SMLM be done in fixed cells.

Generating high spatiotemporal resolution data is particularly challenging due to the resolution-sampling trade-off, which complicates the study of how actin structures influence on protein dynamics at the nanoscale. To address this, we designed our experiment based on a hybrid approach of single-particle tracking followed by

[1]Department of Physics and Astronomy, University of New Mexico, Albuquerque, New Mexico, USA. [2]Department of Pathology, University of New Mexico, Albuquerque, New Mexico, USA. [3]University of New Mexico Comprehensive Cancer Center, Albuquerque, New Mexico, USA. [4]Present address: Lyda Hill Department of Bioinformatics, University of Texas Southwestern Medical Center, Dallas, TX, USA. [5]Present address: Department of Pharmacology, University of Minnesota, Minneapolis, MN, USA. ✉e-mail: hanieh.mazloomfarsibaf@utsouthwestern.edu; klidke@unm.edu

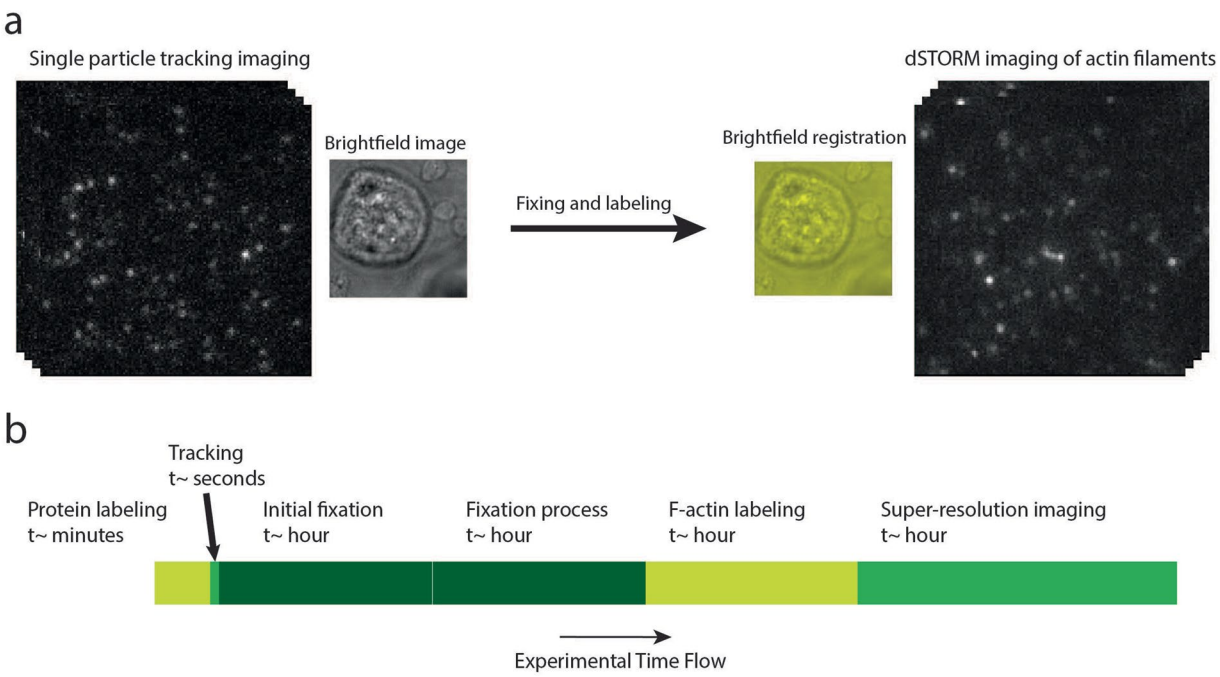

Fig. 1 Experimental workflow for correlative single-particle tracking and super-resolution imaging. (**a**) 2D images of fluorescently labeled IgE receptor protein (left), brightfield image of an RBL cell post-tracking (second from left), overlay of brightfield images post-tracking and pre-super-resolution imaging (second from right), and single-molecule emitters of labeled actin filaments (right). (**b**) Timeline for the entire experiment on a single sample, spanning from a few minutes of tracking to several hours of fixation and labeling for the super-resolution image.

SMLM. This approach was previously implemented by Bálint *et al*. to study cargo transport on microtubules[18]. We customized an optical setup, employing several elegant engineering techniques to integrate single-particle tracking of membrane proteins with super-resolution imaging of actin filaments. We achieved this by optimizing the fixation protocol, ensuring the preservation of cellular morphology throughout the process. We collected two-dimensional time series data in rat basophilic leukemia (RBL-2H3) cells[19] to observe the diffusional dynamics of the transmembrane receptor FcεRI and the outer-leaflet GPI-anchored proteins at high frame rate (490 Hz). Protein mobility was detected in cells with and without treatment to alter actin polymerization. Data collection was performed using TIRF (total internal reflection fluorescence) microscopy to observe only actin structures close to the coverslip, corresponding to the cell membrane.

This data repository can be used for a systematic study on the lateral diffusion of membrane proteins guided by actin structures. The observation of both transmembrane and outer leaflet proteins offers the groundwork for evaluating the direct and indirect interactions of membrane proteins with actin filaments, regulating their dynamics at the nanometer scale. Furthermore, this data repository provides insights into a diverse range of protein dynamics modulated by actin network architectures, depending on specific actin treatments. Upon phalloidin treatment, actin filaments become stabilized, generating more secure corral walls and reducing openings for proteins diffusing into juxtaposed corrals. Phorbol myristate acetate (PMA) induces actin polymerization, forming actin bundles that may have created stiffer barriers between corrals. In summary, this data repository facilitates the exploration of a wide range of mechanisms by which the actin network manipulates the lateral diffusion of membrane proteins.

The proposed optical setup and experimental design are versatile, allowing for an extension of studies requiring rapid dynamics information within the context of ultrastructural details. Our optimized fixation protocol, designed to preserve cellular structures, offers a distinct advantage when transitioning from live-cell imaging to fixed-cell imaging. Of note, this crucial step is frequently overlooked in most literature.

Methods

Experimental Flow of Hybrid Live-Cell and Super-resolution Imaging. We employed a hybrid methodology for data collection using a cost-effective optical system, starting with high-speed live-cell imaging to track individual membrane proteins, which was succeeded by super-resolution imaging of actin filaments of the same cells. Samples were initially treated with specific drugs, tailored to each biological condition, then membrane proteins were labeled for single-particle tracking. Under a carefully designed protocol, cells were fixed and labeled to visualize actin filaments using direct stochastic optical reconstruction microscopy (dSTORM)[20,21] (Fig. 1).

An essential but often overlooked consideration in the literature is the impact of fixation buffer on cell morphology, especially in a hybrid method that includes live-cell imaging, cell fixation, labeling, and dSTORM

imaging. Indeed, maintaining cell integrity through these multiple stages is a challenging aspect of integrated methods. In our dataset, we examined several common and custom fixation protocols concerning the changes in the cell morphology at the microscale, and maintenance of thin actin filaments in super-resolution images. This led us to select glutaraldehyde as the preferred choice and optimize the final concentration by matching the osmolarity with the live-cell imaging buffer (see Technical Validation).

Given the refined protocol and advanced optical setup, our data collection was designed to address two primary inquiries: i) the mechanisms of which actin network architecture guide the transmembrane protein dynamics, and ii) the mechanisms of direct versus indirect interactions of the actin structures that modulate membrane protein dynamics.

Cell culture and live-cell preparation. RBL-2H3 cell lines (ATCC, CRL-2256) were maintained in minimum essential medium (MEM) supplemented with 10% FBS, 1% penicillin streptomycin and 1% L-glutamine[22]. The cells were plated on a 25 mm coverslip (#1.5) mounted in an Attflour cell chamber (Life Technologies, Cat No. A-7816). Samples were prepared differently based on biological conditions as follows:

Class I – Transmembrane protein, FcεRI under actin perturbations. We selected three biological conditions to observe the lateral motion of FcεRI in the context of actin organization: untreated cells, phalloidin-treated cells, and PMA-treated cells. The preparation of untreated and phalloidin-treated samples followed the protocol described in our previous work[23]. Briefly, cells were labeled with Janelia Fluor® 646[24] (Tocris Bioscience, Cat. No. 6148) conjugated to IgE at the final concentration of 150–250 pM diluted in the HANKS buffer for 15 min. The HANKS buffer consisted of 0.9X solution of Hanks Balanced Salt Solution (HBSS) (Invitrogen, SKU#14,065- 056), 10 mM 4-(2-hydroxyethyl) −1-piperazineethanesulfonic acid (HEPES), 5 mM Glucose, 0.7 mM $MgSO_4$, 0.13% $NaHCO_3$ in ddH_2O (HANKS) buffer. Samples were washed once with the HANKS buffer before live-cell imaging. For treated samples, cells were prepared with actin drugs and washed 6x with HANKS buffer before labeling the FcεRI receptors. For phalloidin-treated cells, actin filaments were stabilized by 1 pM of Phalloidin-Alexa 568 (ThermoFisher, Cat No. A12380) in the presence of 0.05% Saponin (Sigma, CAS No. 8047–15–2) diluted in cytoskeleton-preserving buffer (PEM), 80 mM PIPES pH 7.2, 10 mM EGTA, 4 mM MgCl2 (PEM) for 20 s. For PMA-treated cells, samples were pre-incubated for 40 min in 50 nM of PMA diluted in the HANKS buffer at 37 °C.

Class II – Transmembrane protein versus outer leaflet protein. RBL-2H3 cells were transiently transfected using the Amaxa system (Lonza) with Solution L,Program T-20, and 3 μg of plasmid DNA to express a chimeric membrane-anchored GFP-GPI fusion protein[25]. The adequate expression of the GFP-GPI protein was verified using fluorescent microscopy prior to the labeling step. The samples were labeled either for FcεRI receptors with IgE-conjugated Janelia Fluor® 646 or for GPI-anchored proteins with an anti-GFP nanobody conjugated to ATTO 647 N (Chromotek, Cat No. gba647n-10) as described in our previous work[23].

Live- cell imaging and initial fixation. The samples were kept in the HANKS buffer and mounted with a custom designed chamber holder on the stage of the microscope. Single-particle tracking was performed with TIRF illumination with an excitation intensity of ∼1 kW/cm^2 at room temperature. Images were acquired at 490 Hz frame rate (~2 milliseconds exposure time) for a total of 6000 frames. After a few seconds of data acquisition, the initial optimized fixation buffer including the 4% glutaraldehyde diluted in PEM buffer – 80 mM PIPES pH 7.2, 10 mM EGTA, 4 mM MgCl2 – was automatically added in the ratio of 1:1 to the sample with HANKS buffer to have a 2% glutaraldehyde at final concentration (see Technical Validation). A syringe pump was connected to the optical setup and added the buffer at 22 μl/min flow rate. Simultaneously with the fluorescence single-particle tracking, we recorded brightfield images of the cell using an infrared (IR) camera, and continued till the fixation buffer was completely added to the samples. These brightfield images were used for monitoring cell morphology changes during the initial fixation process and for cell image registration before collecting super-resolution images. The cell position at the microscale was manually recorded by noting the stage information of a nanopositioning piezo stage installed on the microscope before removing the sample from the microscope (see Optical Setup section). The samples were removed from the microscope for additional fixation process and labeling the actin filaments.

Cell fixation and actin labeling. After an hour of initial fixation buffer, the samples were washed 2x with phosphate buffer saline (PBS) (gibco, Lot No. 2053546) then kept in fresh prepared $NaBH_4$ for 10 min to reduce background fluorescence due to glutaraldehyde, followed by 2x washes with PBS. To quench reactive cross-linkers, the samples were incubated in 10 mM Tris for 10 min, followed by 2x washes with PBS. Finally, the samples were permeabilized by incubation for 15 min in 5% BSA and 0.05% Triton X-100 diluted in PBS, followed by one PBS wash before labeling actin filaments.

Actin filaments were labeled in fixed cells by incubating them with 0.56 μM AF647-conjugated to phalloidin (ThermoFisher, Cat no. A22287) diluted in PBS for one hour. The samples were washed once in PBS and kept in a dSTORM imaging buffer for super-resolution imaging. This buffer contained an enzymatic oxygen scavenging system and primary thiol: 50 mM tris, 10 mM NaCl, 10% w/v glucose, 168.8 U/ml glucose oxidase (Sigma, Cat No. G2133), 1404 U/ml catalase (Sigma, Cat No. C9322), and 60 mM 2-aminoethanethiol (MEA) (Sigma-Aldrich, Cat no. M6500-25G) with pH 8.0, to optimize chemical conditions for photo-switching of AF647 dye. During data collection, the sample chambers were sealed with a clean 25 mm coverslip to prevent exposure to oxygen.

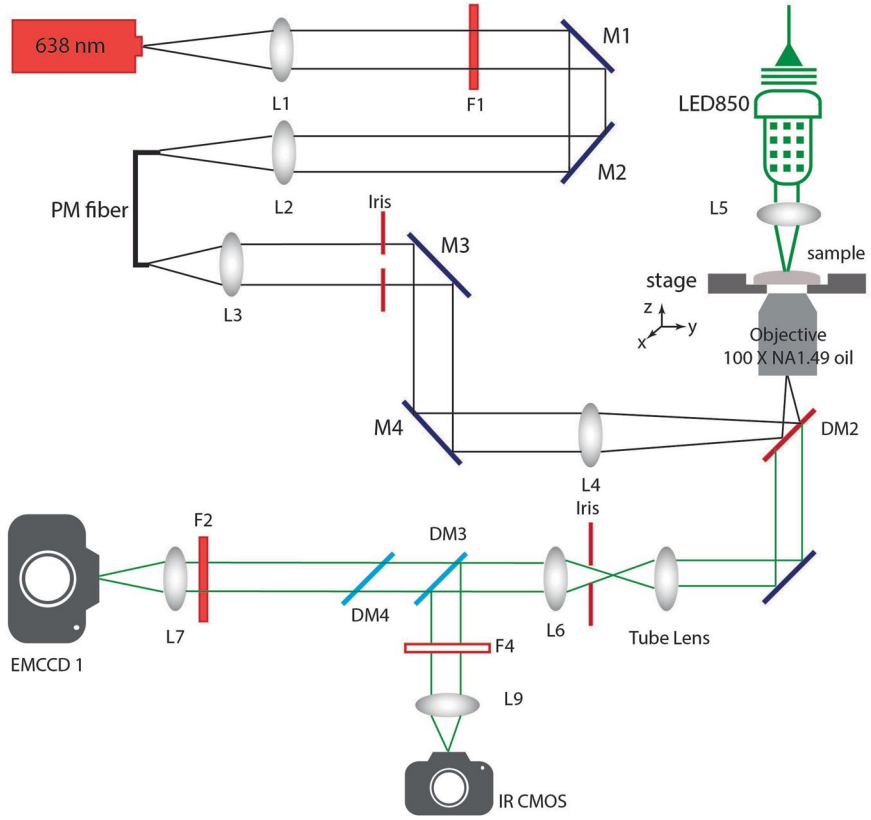

Fig. 2 Optical layout of correlative high-speed single-particle tracking and super-resolution microscope.

Super-resolution imaging. For super-resolution imaging, the samples were carefully remounted onto the microscope. We utilized the IR camera and stage, coupled with the optical setup, to locate the same cell of the live-cell imaging phase. The IR camera, with its wider field of view, captures the cell of interest along with its neighboring cells, facilitating easy cell identification. Meanwhile the field of view of the main camera is limited to a single cell for fast data acquisition in single-particle tracking. The cell position was achieved through a bright-field registration with nanoscale accuracy[26,27]. Only samples with high correlation coefficient with registration threshold of 0.6 were kept for super-resolution imaging. The dSTORM imaging was performed with a 638 nm laser at ~4.7 kW/cm^2 in TIRF illumination with an approximate exposure time of 10 milliseconds. To reduce the possible experimental drifts, such as vibrational and thermal drifts, during data collection, brightfield registration was employed every 3000 frames for actin data collection, as described by Wester, *et al.*[27].

Optical setup. The imaging system was assembled on an inverted microscope (IX71, Olympus America Inc.) equipped with an oil immersion objective lens (Olympus, UAPON 100XOTIRF) (Fig. 2, Table 1) as described in our previous work[28]. For this study, a syringe pump was integrated to automatically deliver the fixation buffer to the samples following single-partible tracking imaging. Briefly, a nanopositioning piezo stage (Mad City Labs, Nano-LPS100) mounted on a two-dimensional manual stage was installed on the microscope for precise cell positioning and brightfield image registration. Brightfield illumination was provided by an 850 nm LED (M850L3, Thorlabs) and images were captured using a low-cost CMOS camera (Thorlabs, DCC1545M) after the light reflected by a short-pass dichroic beam splitter (Semrock, FF750-SDi02) and passed through a single-band band-pass filter (Semrock, FF01-835/70-25). For fluorescent imaging, a 638 nm laser diode (Thorlabs, L638P200) was coupled into a single-mode fiber, reflected by a dichroic beam splitter (Semrock, Di03-R635-t1-25 × 36), and focused onto the back focal plane of the objective lens. Prior to coupling into the fiber, the laser passed through a clean-up filter (Semrock, LD01-640/8). Emission path included a short-pass dichroic beam splitter (Semrock, FF750-SDi02), a single-band bandpass filter (Semrock, FF624-Di01), and an EMCCD camera with a sensor size of 128 × 128 (Andor, iXon DU-860E-CS0-#BV) with a pixel size of 0.1185 µm. Calibration of the EMCCD to extract the effective photon number and offset gave gain at 13 $\frac{e^-}{ADU}$ and offset of 90 ADU[29]. All the instruments were controlled using a custom-written software in MATLAB (MathWorks Inc.)[30].

To measure the illumination pattern on the EMCCD camera, we used a saturated sample of 0.04 µm dark red beads (ThermoFisher, Cat No. F8789), which adhere to the coverslip and are photostable, providing a uniform distribution of the fluorescent molecules in the field of view (Fig. 3a). As shown by a black solid line in Fig. 3b,c, the spatially averaged photon counts are nearly uniform along both the x and y axes of the EMCCD region.

Symbol	Part Number	Description	Vender
Laser 1	L638P200	638 nm, 200 mW, Ø5.6 mm, G Pin Code, Laser Diode	Thorlabs
LED850	M850L3	850 nm, 900 mW (Min) Mounted LED, 1200 mA	Thorlabs
DM1	FF01- 643/20-25	643/20 nm BrightLine@ single-band band-pass filter	Semrock
DM2	Di03-R635-t1-25 × 36	635 nm laser BrightLine@ single-edge super-resolution/TIRF dichroic beamsplitter	Semrock
DM4	FF624-Di01-25 × 36	677 nm edge BrightLine@ single-edge standard epi-fluorescence dichroic beamsplitter	Semrock
L1, L2	A414TM-A	f = 3.30 mm, NA = 0.47 Mounted Rochester Aspheric Lens, AR: 350-700 nm	Thorlabs
L3	LA1560-ML	ML - Ø1/2" N-BK7 Plano-Convex Lens, SM05-Threaded Mount, f = 25.0 mm, Un- coated	Thorlabs
L4	…	f = 175 mm	Thorlabs
L5	AC254-050-A	f = 50.0 mm, Ø1" Achromatic Doublet, ARC:400–700 nm	Thorlabs
L6	AC254-100-A	f = 100.0 mm, Ø1" Achromatic Doublet, ARC: 400–700 nm	Thorlabs
L7	AC254-200-A	f = 200.0 mm, Ø1" Achromatic Doublet, ARC: 400–700 nm	Thorlabs
L9	AC254-050-A	f = 50.0 mm, Ø1" Achromatic Doublet, ARC:400–700 nm	Thorlabs
F1	LD01-640/8	640/8 nm MaxDiodew laser clean-up filter	Semrock
F2		long pass filter 655 nm	
F4	FF01-835/70-25	835/70 nm BrightLine@ single-band band-pass filter	Semrock
M1-M4	BB1-E02	Ø1" Broadband Dielectric Mirror, 400–750 nm	Thorlabs
Iris1,	SM1D12D	SM1 Ring-Actuated Iris Diaphragm (Ø0.8–Ø12 mm)	Thorlabs
Fiber	P1-488PM-FC-2	PM Patch Cable, PANDA, 488 nm, FC/PC, 2 m	Thorlabs

Table 1. Optical component checklist of the correlative high-speed single-tracking and super-resolution microscopy.

Data Records

All image data collected in this study are available in a Zenodo repository[31]. Data was classified as "Class I" and "Class II" describing two categories mentioned in the live-cell preparation section. In "Class II", the cells were transfected to express GFP-GPI-anchored fusion protein. The data with folder names containing "IgE Untreated" include a ".mat" file for image time series of fluorescently labeled IgE receptors in untreated RBL-2H3 cells, and several ".mat" files in the "SRImage" folder containing image series of corresponding super-resolution imaging of fluorescently labeled actin filaments of the same cell. The data with folder names including with "IgE Treated" include a ".mat" file for image time series of fluorescently labeled IgE receptors in either phalloidin- or PMA-treated RBL-2H3 cells, and several ".mat" files in the "SRImage" folder containing image series of corresponding super-resolution imaging of fluorescently labeled actin filaments in the same cell. Similarly, the data with folder names starting with "GPI Untreated" include a ".mat" file of image time series of fluorescently labeled GPI-anchored proteins in untreated RBL-2H3 cells, and several ".mat" files saved in the "SRImage" folder containing image series of corresponding super-resolution imaging of fluorescently labeled actin filaments in the same cell. The data with folder names starting with "GPI Treated" include a ".mat" file of image time series of fluorescently labeled GPI-anchored proteins in phalloidin treated RBL-2H3 cells, and several ".mat" files in the "SRImage" folder containing image series of corresponding super-resolution imaging of fluorescently labeled actin filaments in the same cell. The number within each folder name represents an individual experiment and the corresponding data collected under the same conditions. For all experiments, IR brightfield images were collected to monitor the cell morphology during live-cell image and adding initial fixation buffer and were saved in the tracking file. A single IR brightfield image for cell registration and drift correction during super-resolution imaging was saved in the "SRImage" folder for each cell.

Data for the Technical Validation section are saved in a separate folder named 'TechnicalValidation'. This folder includes 'IRMovies', a set of brightfield IR images of the cell during tracking and adding various fixation buffers, according to Table 2.

We have updated the Zenodo repository to include the HDF5 files containing tracking data and super-resolution images for each sample[31]. The files are named "Tracking" and "SuperResoulution_actin" within their respective folders corresponding to the experimental conditions mentioned above. The "Technical Validation" folder in updated version includes the "IRMovies" files, a set of brightfield IR images capturing the full field of view from the IR camera that contained several cells for each fixation buffer, as outlined in Table 2.

Technical Validation

Fixation buffer optimization. For an integrated live- and fixed-cell imaging method, the chemical fixation protocol must be optimized to preserve the morphologies and physical properties of a sample at the living state[32,33]. In single-cell imaging, the standard fixation protocol is an aldehyde-based buffer including paraformaldehyde (PFA) and glutaraldehyde (GA) which react with the amino group and form cross-links between membrane proteins and their surroundings[34,35]. Recently, glyoxal has been also considered as an alternative fixative in super-resolution imaging[36]. Most fixation methods significantly affect cell morphology and tissue architecture[37,38]. Therefore, in this study, we optimized the fixation protocol by testing different concentrations of standard buffers in respect to (1) an isotonic fixation buffer matching to live-cell imaging buffer, (2) the unchanged cell morphology at the microscale, (3) high super-resolved images of actin filaments.

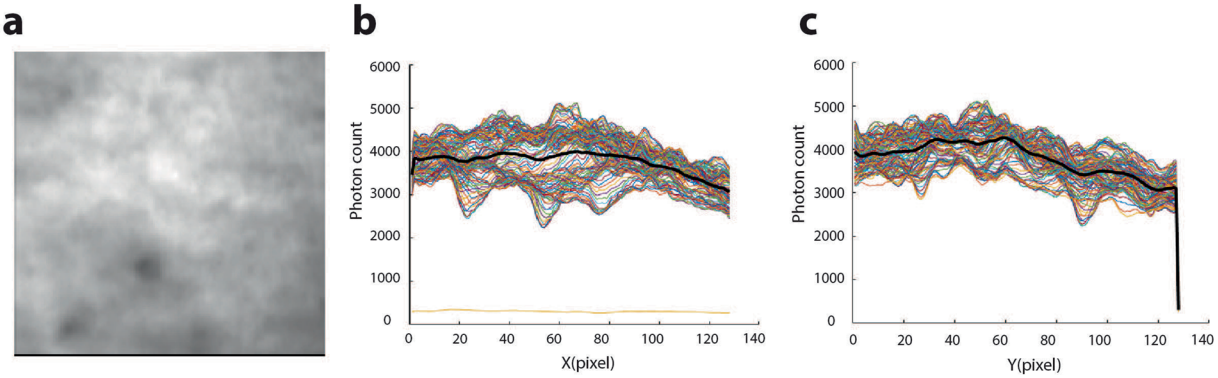

Fig. 3 Fluorescent image of a saturated 0.04 µm dark red bead sample used for testing the illumination pattern with a 638 nm light source. (**a**) Frame-averaged raw image of the saturated sample captured on the EMCCD camera. Photon counts for each (**b**) row (x direction) and (**c**) column (y direction) are plotted. The black line is the average photon counts across all (**b**) rows and (**c**) columns.

File name	Experimental conditions
IRMovie 1	HANKS
IRMovie 2	4% PFA in PEM
IRMovie 3	2% GA in PEM
IRMovie 4	2% GA + 0.1% Triton in PEM
IRMovie 5	2% GA + 0.2% Triton in PEM
IRMovie 6	3% Glyoxal + 20% Ethanol in DI water
IRMovie 7	1.5% Glyoxal + 10% Ethanol in DI water
IRMovie 8	3% Glyoxal in DI water
IRMovie 9	1.2% PFA in PEM
IRMovie 10	0.6% PFA in PEM
IRMovie 11	0.4% PFA in PEM

Table 2. Concentration of fixation buffers for examining cellular morphology changes using IR brightfield images, corresponding to the Technical Validation IRMovie data in the data repository.

Buffer	DI Water	PBS	PEM
2% GA	0.2	0.474	0.3
2% GA + 0.1% Triton	0.201	0.476	0.3
0.6% PFA + 0.1% GA + 0.25% Triton	0.213	0.489	0.316
3% Glyoxal + 30% Ethanol	7.15	----	----
PBS	0.275	----	----
PEM	0.102	----	----
HANKS	0.307	----	----

Table 3. Osmolarity (Osm/L) of chemical fixation buffer. PEM is the cytoskeleton-preserving buffer consisting of 80 mM PIPES, 5 mM EGTA, and 2 mM $MgCl_2$. HANKS buffer is a live-cell imaging buffer which keeps the cells in a healthy condition.

Osmolarity. We eliminated osmotic responses of the cell by matching the osmolarity of the optimized fixation buffer with the live-cell imaging buffer. In each fixation procedure, various concentrations of PFA, GA, or glyoxal (40% stock solution from Sigma-Aldrich, #128465) were diluted in deionized (DI) water, PBS, or cytoskeleton preserving buffer (PEM) (Table 3). Considering the factors mentioned in the following sections, we chose 2% GA in the PEM buffer as an optimized fixation buffer for this study.

IR Movies while adding fixation buffer. During live-cell imaging and adding the fixation buffer, we monitored cell morphology using the IR camera. For each fixation procedure, we captured a time series of brightfield images while adding the fixation buffer to the HANKS buffer with the syringe pump (Table 2). The cross-correlation coefficient was calculated using the 'corr2' function in MATLAB, with the first image as the

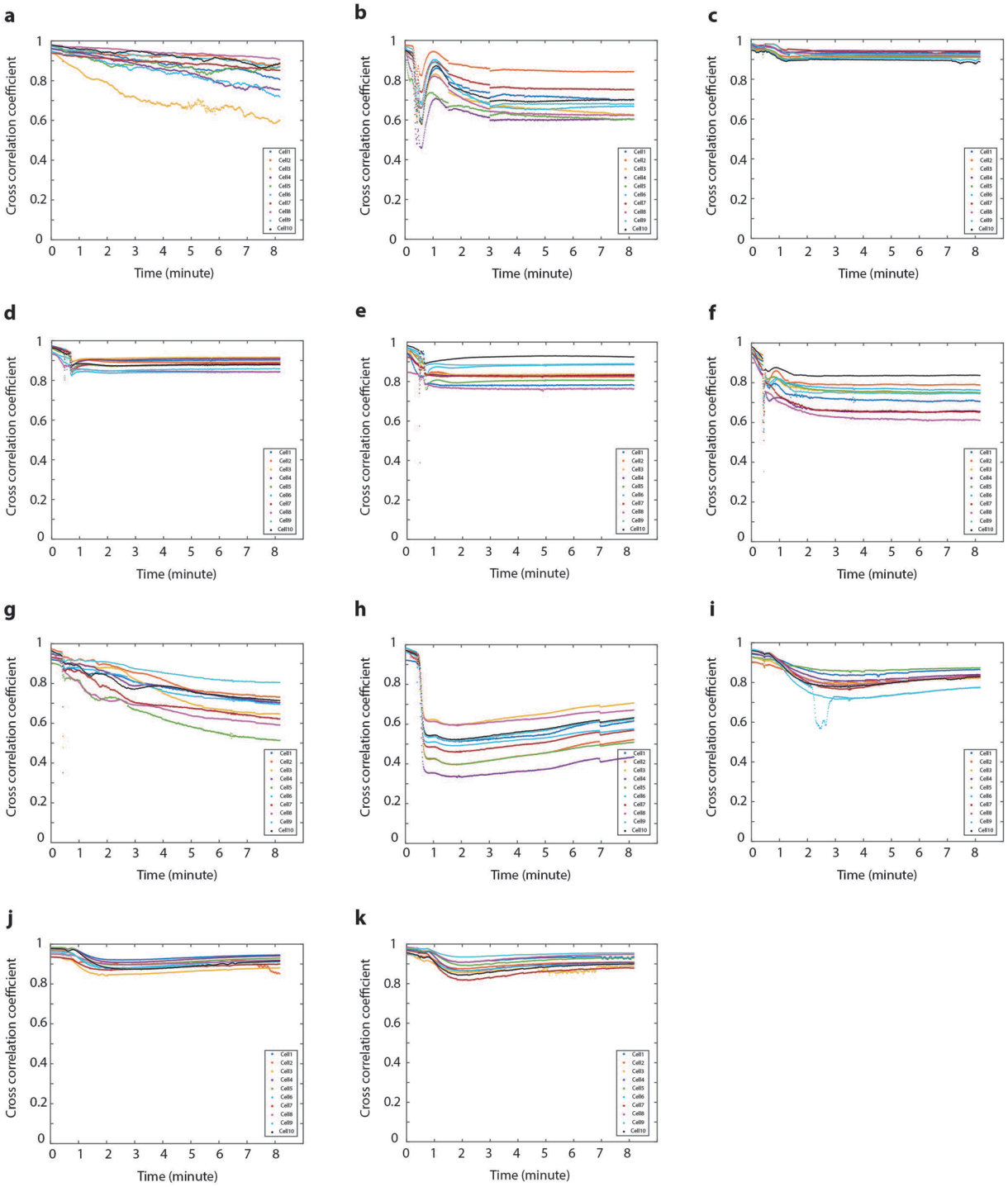

Fig. 4 Correlation coefficient of IR brightfield images under various fixation buffers. Ten cells are selected to observe cell morphology changes using IR brightfield images as different fixation buffers were added to the HANKS buffer: (**a**) HANKS, (**b**) 4% PFA in PEM, (**c**) 2% GA in PEM, (**d**) 2% GA + 0.1% Triton in PEM, (**e**) 2% GA + 0.2% Triton in PEM, (**f**) 3% glyoxal + 20% ethanol in DI water, (**g**) 1.5% glyoxal + 10% ethanol in DI water, (**h**) 3% glyoxal in DI water, (**i**) 1.2% PFA in PEM, (**j**) 0.6% PFA in PEM, and (**k**) 0.4% PFA in PEM.

reference image. This analysis was performed for the entire time series of the brightfield images for 10 selected cells per condition (Fig. 4). The IR brightfield images are available on the Zenodo repository[31].

Super-resolved images of actin filaments. The quality of super-resolution images relies on well-executed sample preparation, including the fixation protocol which depends on targeted structures. For optimizing the fixation buffer, we visualized the actin structures for the GA-based fixation buffers that preserve

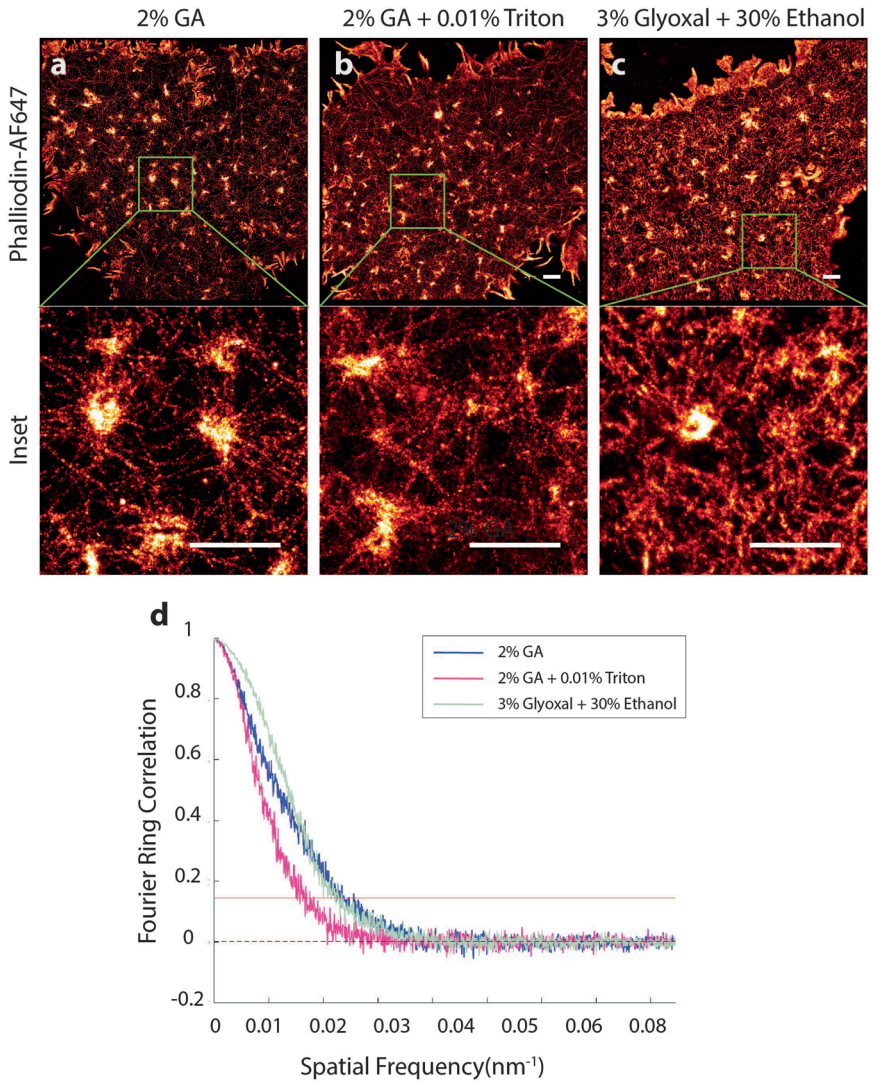

Fig. 5 Super-resolution images of actin filaments labeled with phalloidin-AF647 in RBL-2H3 cells. The immediate fixation buffers used are (**a**) 2% GA in PEM, (**b**) 2% GA with 0.1% Triton in PEM, and (**c**) 3% glyoxal with 20% ethanol in DI water. Scale bar is one µm. (**d**) FRC curve for the super-resolution images of actin filaments. The horizontal red line at FRC = 1/7 indicates the threshold of the curve, where the image resolution is defined as the inverse of the spatial frequency.

cell morphology at the microscale, as imaged with the IR camera in the previous section. We also examined a glyoxal-based fixation buffer as suggested by Richter *et al.*, which is particularly effective for actin structures[36].

Three fixation protocols were evaluated: i) 2% GA in PEM, ii) 2% GA with 0.1% Triton in PEM, and iii) 3% glyoxal with 20% Ethanol in DI water. These buffers were used as the immediate fixation step, followed the remaining fixation steps detailed in the Methods section. Actin filaments were labeled with AF647-conjugated to phalloidin. We generated super-resolution images of actin structures using a custom-written Single Molecule Imaging Toolbox Extraordinaire (SMITE)[39] (see Usage note). To quantify the spatial resolution of actin filaments, we employed the Fourier Ring Correlation (FRC)[17], an image-based metric (Fig. 5). As shown in the FRC curves (Fig. 5d), the average spatial resolution of actin filaments achieved with the three fixation buffers was 42.8 nm, 60.2 nm, and 44.1 nm, respectively. This confirmed that 2% GA in PEM buffer is a well-chosen fixation buffer.

In addition to testing for the fixation buffer, we collected the super-resolved images of actin filaments to observe whether phalloidin and PMA treatment have any significant impacts on the actin filaments visualization. For all untreated and treated experimental conditions, we provided super-resolution images of actin structures along with corresponding tracking data[31].

Usage Note

To demonstrate the usage of this dataset, we analyzed a sample using the Single Molecule Imaging Toolbox Extraordinaire (SMITE) package[39], a custom-written MATLAB tool combined with the DIPimage toolbox[40]. Specifically, we utilized the "ClassII_IgEPhalloidin_Treated1" dataset from the Zenodo repository[31].

For two-dimensional images, single emitters were localized as individual spots, described by parameters such as positions, total photon counts, background photon counts and their standard errors. These parameters were

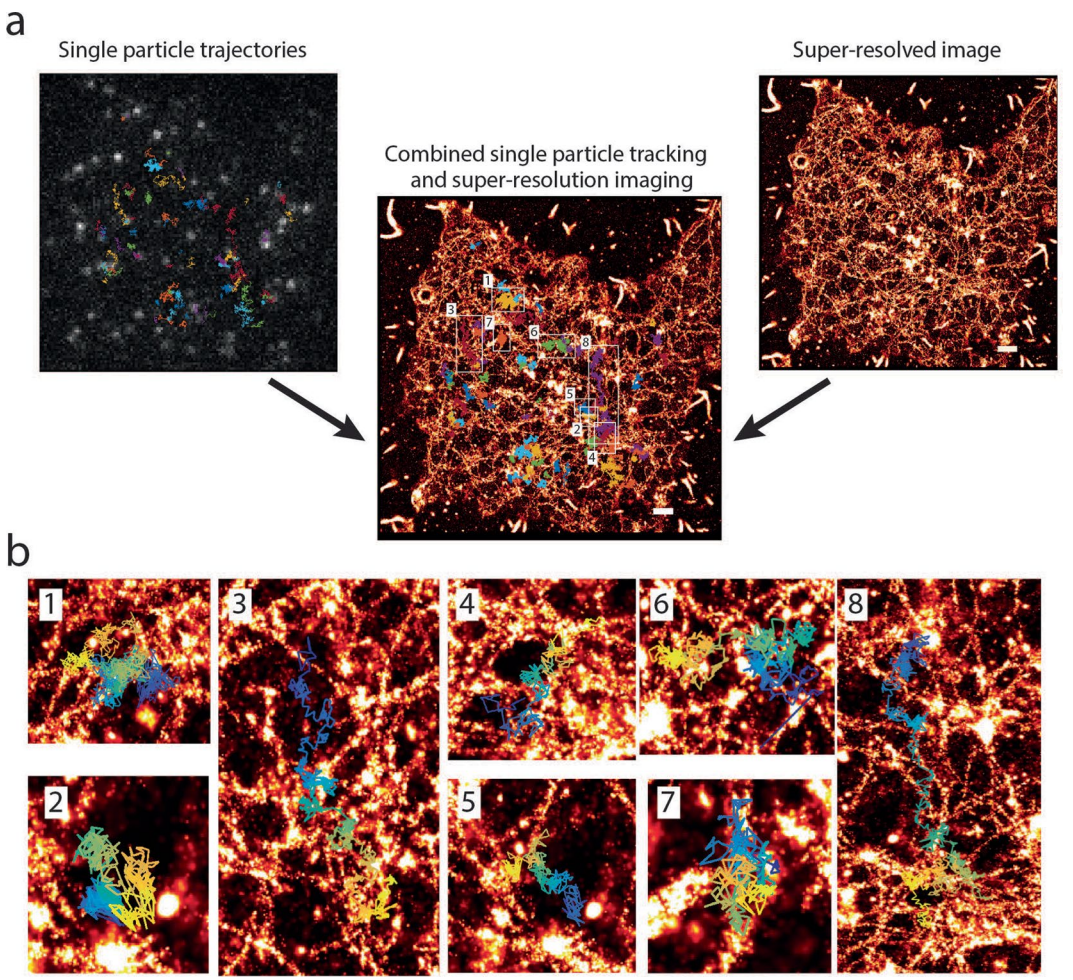

Fig. 6 Analysis of high-speed single-particle tracking of membrane proteins combined with super-resolution imaging of actin filaments in an RBL-2H3 cell. (**a**) Trajectories of IgE receptors obtained from single-particle tracking images, with each trajectory represented by a different color (left). Super-resolved image of actin filaments in the same cell (right). Overlay of single- particle trajectories with super-resolved image (middle). Scale bar is one μm. (**b**) Close-up of super-resolved images of actin filaments surrounding selected trajectories in specific regions. The color gradient of each trajectory represents the passage of time, transitioning from earlier stages (blue) to later stages (yellow).

computed using a maximum likelihood estimator implemented on a graphics processing unit (GPU)[41]. Using the 'SMLM' module in the SMITE package for super-resolution image of actin filaments, we applied thresholds to refine data: a maximum background photon counts of 200, a minimum photon counts per frame per emitter of 200, and a data-model hypothesis test[42] with a p-value cutoff of 0.01. The PSF sigma for fitting a Gaussian model to localize emitters was set to 1.14 pixels. These parameters resulted in a well-defined set of single molecule localizations. To generate a super-resolution image of actin filaments, we reconstructed this refined localization set was reconstructed (Fig. 6). For single-particle tracking, trajectories of individual membrane proteins were generated using a tracking algorithm based on a linear assignment problem and a cost matrix proposed by Jaqaman *et al.*[39,43] (Fig. 6).

We assessed the position accuracy of emitters for single-particle tracking under different experimental conditions using a custom MATLAB code, as described in Schwartz *et al.*[41,44,45]. For Janelia Fluor 646 conjugated to IgE receptors, the median position accuracy of localized molecules was estimated at 18.78 nm, 16.25 nm, and 17.41 nm for untreated cells, phalloidin-treated cells, and PMA-treated cells in the Class I dataset, respectively. In the Class II dataset, the median position accuracy was 17.30 nm for Janelia Fluor 646 conjugated to IgE receptors, while anti-GFP ATTO 647 N conjugated nanobody had an estimated accuracy of 21.26 nm, and 22.27 nm for untreated and phalloidin-treated cells, respectively.

Code availability

All instruments of our optical system were controlled by a MATLAB-based custom-written package[30], which is freely available at (github.com/LidkeLab/matlab-instrument-control).

Received: 22 August 2024; Accepted: 7 March 2025;
Published online: 03 April 2025

References

1. Cho, W. & Stahelin, R. V. Membrane-protein interactions in cell signaling and membrane trafficking. *Annu Rev Biophys Biomol Struct* **34**, 119–151, https://doi.org/10.1146/annurev.biophys.33.110502.133337 (2005).
2. Escriba, P. V. *et al*. Membranes: a meeting point for lipids, proteins and therapies. *J Cell Mol Med* **12**, 829–875, https://doi.org/10.1111/j.1582-4934.2008.00281.x (2008).
3. Jaqaman, K. & Ditlev, J. A. Biomolecular condensates in membrane receptor signaling. *Curr Opin Cell Biol* **69**, 48–54, https://doi.org/10.1016/j.ceb.2020.12.006 (2021).
4. Israelachvili, J. N., Marcelja, S. & Horn, R. G. Physical principles of membrane organization. *Q Rev Biophys* **13**, 121–200, https://doi.org/10.1017/s0033583500001645 (1980).
5. Kusumi, A., Sako, Y. & Yamamoto, M. Confined Lateral Diffusion of Membrane-Receptors as Studied by Single-Particle Tracking (Nanovid Microscopy) - Effects of Calcium-Induced Differentiation in Cultured Epithelial-Cells. *Biophysical Journal* **65**, 2021–2040, https://doi.org/10.1016/S0006-3495(93)81253-0 (1993).
6. Ritchie, K., Iino, R., Fujiwara, T., Murase, K. & Kusumi, A. The fence and picket structure of the plasma membrane of live cells as revealed by single molecule techniques (Review). *Mol Membr Biol* **20**, 13–18, https://doi.org/10.1080/0968768021000055698 (2003).
7. Kusumi, A. *et al*. Dynamic Organizing Principles of the Plasma Membrane that Regulate Signal Transduction: Commemorating the Fortieth Anniversary of Singer and Nicolson's Fluid-Mosaic Model. *Annu Rev Cell Dev Bi* **28**, 215–250, https://doi.org/10.1146/annurev-cellbio-100809-151736 (2012).
8. Kusumi, A. *et al*. Paradigm shift of the plasma membrane concept from the two-dimensional continuum fluid to the partitioned fluid: High-speed single-molecule tracking of membrane molecules. *Annu Rev Bioph Biom* **34**, 351–U354, https://doi.org/10.1146/annurev.biophys.34.040204.144637 (2005).
9. Ritchie, K. *et al*. Detection of non-Brownian diffusion in the cell membrane in single molecule tracking. *Biophysical Journal* **88**, 2266–2277, https://doi.org/10.1529/biophysj.104.054106 (2005).
10. Andrade, D. M. *et al*. Cortical actin networks induce spatio-temporal confinement of phospholipids in the plasma membrane–a minimally invasive investigation by STED-FCS. *Sci Rep-Uk* **5**, 11454 (2015).
11. Dinic, J., Ashrafzadeh, P. & Parmryd, I. Actin filaments attachment at the plasma membrane in live cells cause the formation of ordered lipid domains. *Bba-Biomembranes* **1828**, 1102–1111, https://doi.org/10.1016/j.bbamem.2012.12.004 (2013).
12. Fujiwara, T., Ritchie, K., Murakoshi, H., Jacobson, K. & Kusumi, A. Phospholipids undergo hop diffusion in compartmentalized cell membrane. *Journal of Cell Biology* **157**, 1071–1081, https://doi.org/10.1083/jcb.200202050 (2002).
13. Goswami, D. *et al*. Nanoclusters of GPI-Anchored Proteins Are Formed by Cortical Actin-Driven Activity. *Cell* **135**, 1085–1097, https://doi.org/10.1016/j.cell.2008.11.032 (2008).
14. Plowman, S. J., Muncke, C., Parton, R. G. & Hancock, J. F. H-ras, K-ras, and inner plasma membrane raft proteins operate in nanoclusters with differential dependence on the actin cytoskeleton. *P Natl Acad Sci USA* **102**, 15500–15505, https://doi.org/10.1073/pnas.0504114102 (2005).
15. Andrews, N. L. *et al*. Actin restricts FcεRI diffusion and facilitates antigen-induced receptor immobilization. *Nature Cell Biology* **10**, 955–963, https://doi.org/10.1038/ncb1755 (2008).
16. Sadegh, S., Higgins, J. L., Mannion, P. C., Tamkun, M. M. & Krapf, D. Plasma membrane is compartmentalized by a self-similar cortical actin meshwork. *Phys Rev X* **7**, 011031 (2017).
17. Nieuwenhuizen, R. P. J. *et al*. Measuring image resolution in optical nanoscopy. *Nature Methods* **10**, 557−+, https://doi.org/10.1038/Nmeth.2448 (2013).
18. Bálint, S., Vilanova, I. V., Alvarez, A. S. & Lakadamyali, M. Correlative live-cell and superresolution microscopy reveals cargo transport dynamics at microtubule intersections. *P Natl Acad Sci USA* **110**, 3375–3380, https://doi.org/10.1073/pnas.1219206110 (2013).
19. Passante, E. & Frankish, N. The RBL-2H3 cell line: its provenance and suitability as a model for the mast cell. *Inflamm Res* **58**, 737–745, https://doi.org/10.1007/s00011-009-0074-y (2009).
20. Endesfelder, U. & Heilemann, M. Direct stochastic optical reconstruction microscopy (d STORM). *Advanced Fluorescence Microscopy: Methods and Protocols*, 263–276 (2015).
21. Heilemann, M. *et al*. Subdiffraction-resolution fluorescence imaging with conventional fluorescent probes. *Angew Chem Int Edit* **47**, 6172–6176, https://doi.org/10.1002/anie.200802376 (2008).
22. Wilson, B. S., Pfeiffer, J. R. & Oliver, J. M. Observing FcepsilonRI signaling from the inside of the mast cell membrane. *J Cell Biol* **149**, 1131–1142, https://doi.org/10.1083/jcb.149.5.1131 (2000).
23. Mazloom-Farsibaf, H., Kanagy, W. K., Lidke, D. S. & Lidke, K. A. High-speed single molecule imaging datasets of membrane proteins in rat basophilic leukemia cells. *Data Brief* **30**, 105424, https://doi.org/10.1016/j.dib.2020.105424 (2020).
24. Grimm, J. B., Brown, T. A., English, B. P., Lionnet, T. & Lavis, L. D. Synthesis of Janelia Fluor HaloTag and SNAP-Tag Ligands and Their Use in Cellular Imaging Experiments. *Methods Mol Biol* **1663**, 179–188, https://doi.org/10.1007/978-1-4939-7265-4_15 (2017).
25. Sharma, P. *et al*. Nanoscale organization of multiple GPI-anchored proteins in living cell membranes. *Cell* **116**, 577–589, https://doi.org/10.1016/S0092-8674(04)00167-9 (2004).
26. Valley, C. C., Liu, S., Lidke, D. S. & Lidke, K. A. Sequential superresolution imaging of multiple targets using a single fluorophore. *PloS one* **10**, e0123941 (2015).
27. Wester, M. J. *et al*. Robust, fiducial-free drift correction for super-resolution imaging. *Sci Rep-Uk* **11**, 23672 (2021).
28. Mazloom-Farsibaf, H. *et al*. Comparing lifeact and phalloidin for super-resolution imaging of actin in fixed cells. *PLoS One* **16**, e0246138 (2021).
29. Van Vliet, L. J., Sudar, D. & Young, I. T. Digital fluorescence imaging using cooled CCD array cameras invisible. *Cell Biol* **3**, 109–120 (1998).
30. Pallikkuth, S. *et al*. A MATLAB-based Instrument Control Package for Fluorescence Imaging. *Biophysical Journal* **114**, 532a–532a, https://doi.org/10.1016/j.bpj.2017.11.2912 (2018).
31. Mazloom-Farsibaf, H. *Data Repository: Correlative High-Speed Single Particle Tracking of Membrane Proteins and Super-resolution Microscopy of Actin Zenodo* https://doi.org/10.5281/zenodo.14284882 (2024).
32. Kim, S.-O., Kim, J., Okajima, T. & Cho, N.-J. Mechanical properties of paraformaldehyde-treated individual cells investigated by atomic force microscopy and scanning ion conductance microscopy. *Nano Converg* **4**, 1–8 (2017).
33. Schnell, U., Dijk, F., Sjollema, K. A. & Giepmans, B. N. G. Immunolabeling artifacts and the need for live-cell imaging. *Nature Methods* **9**, 152–158, https://doi.org/10.1038/Nmeth.1855 (2012).
34. Leyton-Puig, D. *et al*. PFA fixation enables artifact-free super-resolution imaging of the actin cytoskeleton and associated proteins. *Biol Open* **5**, 1001–1009, https://doi.org/10.1242/bio.019570 (2016).
35. McLean, I. W. & Nakane, P. K. Periodate-lysine-paraformaldehyde fixative. A new fixation for immunoelectron microscopy. *J Histochem Cytochem* **22**, 1077–1083, https://doi.org/10.1177/22.12.1077 (1974).
36. Richter, K. N. *et al*. Glyoxal as an alternative fixative to formaldehyde in immunostaining and super-resolution microscopy. *Embo J* **37**, 139–159, https://doi.org/10.15252/embj.201695709 (2018).
37. Paavilainen, L. *et al*. The Impact of Tissue Fixatives on Morphology and Antibody-based Protein Profiling in Tissues and Cells. *Journal of Histochemistry & Cytochemistry* **58**, 237–246, https://doi.org/10.1369/jhc.2009.954321 (2010).

38. Srinivasan, M., Sedmak, D. & Jewell, S. Effect of fixatives and tissue processing on the content and integrity of nucleic acids. *Am J Pathol* **161**, 1961–1971, https://doi.org/10.1016/S0002-9440(10)64472-0 (2002).
39. Schodt, D. *et al*. SMITE (single molecule imaging toolbox extraordinaire), a MATLAB package. *Biophysical Journal* **122**, 275a–275a (2023).
40. Hendriks, C. L., van Vliet, L., Rieger, B. & van Ginkel, M. DIPimage: a scientific image processing toolbox for MATLAB, 1999. *Pattern Recognition Group, Department of Applied Physics, Delft University of Technology*, http://www.ph.tn.tudelft.nl/DIPlib (2018).
41. Smith, C. S., Joseph, N., Rieger, B. & Lidke, K. A. Fast, single-molecule localization that achieves theoretically minimum uncertainty. *Nature Methods* **7**, 373–U352, https://doi.org/10.1038/Nmeth.1449 (2010).
42. Huang, F., Schwartz, S. L., Byars, J. M. & Lidke, K. A. Simultaneous multiple-emitter fitting for single molecule super-resolution imaging. *Biomed Opt Express* **2**, 1377–1393, https://doi.org/10.1364/Boe.2.001377 (2011).
43. Jaqaman, K. *et al*. Robust single-particle tracking in live-cell time-lapse sequences. *Nature Methods* **5**, 695–702, https://doi.org/10.1038/nmeth.1237 (2008).
44. Schwartz, S. L. *et al*. Differential mast cell outcomes are sensitive to FcepsilonRI-Syk binding kinetics. *Mol Biol Cell* **28**, 3397–3414, https://doi.org/10.1091/mbc.E17-06-0350 (2017).
45. Ober, R. J., Ram, S. & Ward, E. S. Localization accuracy in single-molecule microscopy. *Biophysical Journal* **86**, 1185–1200, https://doi.org/10.1016/S0006-3495(04)74193-4 (2004).

Acknowledgements

The work in this paper was primarily supported by NIH/NIGMS grants R01GM109888, 5P50GM085273, and R35GM126934. KAL was additionally supported by NIH/NIGMS grant 1R01GM140284. This work was conducted with support from the University of New Mexico Office of the Vice President for Research Program for Enhancing Research Capacity. We also thank Shayna Lucero for assistance with cell culture and Derek Rinaldi for conjugating IgE to Janelia Fluor® 646.

Author contributions

K.A.L. and H.M. conceived and designed the project. K.A.L. supervised the project. H.M. designed and built the optical setup and collected data for all experimental conditions. K.L.A. and H.M. wrote the codes for controlling the microscope. W.K.K. performed the GFP-transfection cells, and D.S.L. and W.K.K. assisted with the biological insights and sample preparation. H.M. wrote the manuscript. K.A.L., D.S.L. and W.K.K. contributed to writing and editing the manuscript. All authors read and approved of the final manuscript.

Competing interests

The authors declare no competing interests.

Additional information

Correspondence and requests for materials should be addressed to H.M.-F. or K.A.L.